Ecological Dynamics of Broad- and Narrow-Host-Range Viruses Infecting the Bloom-Forming Toxic Cyanobacterium Microcystis aeruginosa

AUTHOR(S):

Morimoto, Daichi; Yoshida, Naohiro; Sasaki, Aya; Nakagawa, Satoshi; Sako, Yoshihiko; Yoshida, Takashi

CITATION:

Morimoto, Daichi ...[et al]. Ecological Dynamics of Broad- and Narrow-Host-Range Viruses Infecting the Bloom-Forming Toxic Cyanobacterium Microcystis aeruginosa. Applied and Environmental Microbiology 2023, 89(2): e02111-22.

ISSUE DATE:

2023-02-28

URL:

http://hdl.handle.net/2433/279506

AMERICAN SOCIETY FOR MICROBIOLOGY | Applied and Environmental Microbiology®

ENVIRONMENTAL MICROBIOLOGY

Ecological Dynamics of Broad- and Narrow-Host-Range Viruses Infecting the Bloom-Forming Toxic Cyanobacterium *Microcystis aeruginosa*

Daichi Morimoto,[a] Naohiro Yoshida,[a] Aya Sasaki,[a] Satoshi Nakagawa,[a] Yoshihiko Sako,[a] Takashi Yoshida[a]

[a]Graduate School of Agriculture, Kyoto University, Kyoto, Japan

ABSTRACT *Microcystis aeruginosa* is predicted to interact and coexist with diverse broad- and narrow-host-range viruses within a bloom; however, little is known about their affects on *Microcystis* population dynamics. Here, we developed a real-time PCR assay for the quantification of these viruses that have different host ranges. During the sampling period, total *Microcystis* abundance showed two peaks in May and August with a temporary decrease in June. The *Microcystis* population is largely divided into three phylotypes based on internal transcribed sequences (ITS; ITS types I to III). ITS I was the dominant phylotype (66% to 88%) except in June. Although the ITS II and III phylotypes were mostly less abundant, these phylotypes temporarily increased to approximately equivalent abundances of the ITS I population in June. During the same sampling period, the abundances of the broad-host-range virus MVGF_NODE331 increased from April to May and from July to October with a temporary decrease in June, in which its dynamics were in proportion to the increase of total *Microcystis* abundances regardless of changes in host ITS population composition. In contrast, the narrow-host-range viruses MVG_NODE620 and Ma-LMM01 were considerably less abundant than the broad-host-range virus and generally did not fluctuate in the environment. Considering that *M. aeruginosa* could increase the abundance and sustain the bloom under the prevalence of the broad-host-range virus, host abundant and diverse antiviral mechanisms might contribute to coexistence with its viruses.

IMPORTANCE The bloom-forming toxic cyanobacterium *Microcystis aeruginosa* interacts with diverse broad- and narrow-host-range viruses. However, the dynamics of the *Microcystis* population (at the intraspecies level) and viruses with different host ranges remain unknown. Our real-time PCR assays unveiled that the broad-host-range virus gradually increased in abundance over the sampling period, in proportion to the increase in total *Microcystis* abundance regardless of changes in genotypic composition. The narrow-host-range viruses were considerably less abundant than the broad-host-range virus and did not generally fluctuate in the environment. The expansion and maintenance of the *Microcystis* bloom even under the increased infection by the broad-host-range virus suggested that highly abundant and diverse antiviral mechanisms allowed them to coexist with viruses under selective pressure. This paper expands our knowledge about the ecological dynamics of *Microcystis* viruses and provides potential insights into their coexistence with their host.

KEYWORDS *Microcystis aeruginosa*, cyanophages, real-time PCR, amplicon sequencing, internal transcribed spacers, cyanobacterial bloom

Microcystis aeruginosa is one of the most pervasive and harmful cyanobacteria that can accumulate at the surface of the water, leading to the development of massive dense blooms in eutrophic freshwater ecosystems (1). Some *Microcystis* strains can produce the potent hepatotoxin microcystin (2–4), and thus their toxic blooms have

Editor Nicole R. Buan, University of Nebraska-Lincoln

Address correspondence to Takashi Yoshida, yoshida.takashi.7a@kyoto-u.ac.jp.

The authors declare no conflict of interest.

Received 15 December 2022
Accepted 4 January 2023
Published 23 January 2023

caused fatal accidents for livestock, pets, and wildlife (5). *Microcystis* toxicity also poses serious problems for humans who use impaired water resources for dialysis treatment (6). Therefore, the World Health Organization proposes a drinking water guideline of 1 μg/L for microcystin (7). Thus, it is a global issue for maintaining safe water supplies to identify and characterize the environmental and biological factors that affect *Microcystis* abundance and composition (8).

One of the most unique features of *M. aeruginosa* is that they possess highly abundant and diverse antiviral defense systems in the genome (9–11). *Microcystis* CRISPR-based studies have revealed that blooms are composed of diverse populations with different CRISPR spacers acquired from foreign DNA fragments (12–14), suggesting that *M. aeruginosa* has frequently interacted with diverse viruses in the environment. Consistent with this observation, the number of *Microcystis* viral isolates has been gradually increasing since Ma-LMM01 was first isolated (e.g., MaMV-DC, PhiMa05, Mic1, Me-ZS1, ΦMHI42, Mwe-Yong1112-1, and Mae-Yong1326-1) (15–22). In addition to these isolates, we recently revealed the existence of *Microcystis* viruses classified into groups I (including Ma-LMM01), II, and III through a metagenomic approach (23). Based on the phylogenetic distribution of host strains with spacers against each group, *Microcystis* group II viruses are predicted to have a broad host range, whereas the group I and III viruses have a narrow host range (23). Indeed, the narrow host ranges of Ma-LMM01 and newly isolated Mic1 (15, 18, 24), each of which corresponds to the group I and III virus, corroborate the validity of our *in silico* predictions, although there was no direct evidence of group II viral host range because of the lack of corresponding viral isolates. Furthermore, it was recently shown that a novel siphovirus with high similarity to prophage-like sequences in *M. aeruginosa* NIES-88 existed in the environment (25).

Among these *Microcystis* viruses, the ecological dynamics of Ma-LMM01 have been intensively studied by quantification of *gp091* (tail sheath) abundance (26). For example, previous studies revealed that a clear increase in Ma-LMM01 abundance was observed at the same time as total *Microcystis* abundance decreased (27) and that Ma-LMM01 infection was likely to occur in 0.01 to 2.9 cells/mL of the natural *Microcystis* population (28). The latter observation reflects the narrow host range of Ma-LMM01; this virus might have the potential to infect only a small part of the *Microcystis* population in the natural environment. Furthermore, the metatranscriptome approach in Lake Tai indicated the negative correlation between *gp091* and lysogenic-associated genes, creating a debate on the existence of a lysogenic state for Ma-LMM01 (29). In contrast, our knowledge about the ecological dynamics of other phylogenetically different *Microcystis* viruses is limited to only a few studies conducted in Lake Erie and Lake Taihu (25, 30). Of these, the latter study based on RNA polymerase sequence (*rpoB*) demonstrated that *Microcystis* myovirus and siphovirus were positively correlated with host populations, including several morphospecies, that emerged in the early and late bloom, respectively (25). However, little is known about the relationships between the ecological dynamics of *Microcystis* population at the intraspecies level and those of its viruses with different host ranges.

In this study, we developed a real-time quantitative PCR (qPCR) assay to monitor the environmental dynamics of broad- and narrow-host-range *Microcystis* viruses. Furthermore, we investigated *Microcystis* population dynamics based on ITS type to assess the relevance of each viral type dynamics on the bloom during the same sampling period.

RESULTS

Seasonal changes in total and ITS phylotype abundances of *M. aeruginosa*. Dense *Microcystis* blooms have occurred at Hirosawanoike Pond every year because of the eutrophication caused by nutrient influx from agricultural fields (28, 31, 32). We first investigated the total abundance of *M. aeruginosa* from May to October 2016. The phycocyanin intergenic spacer (PC-IGS) gene copy numbers of *M. aeruginosa* significantly increased from 4.64×10^4 copies/mL in May to 1.51×10^7 copies/mL in August (*P* value, 0.021 by Tukey-Kramer test) and then decreased in October (1.39×10^6

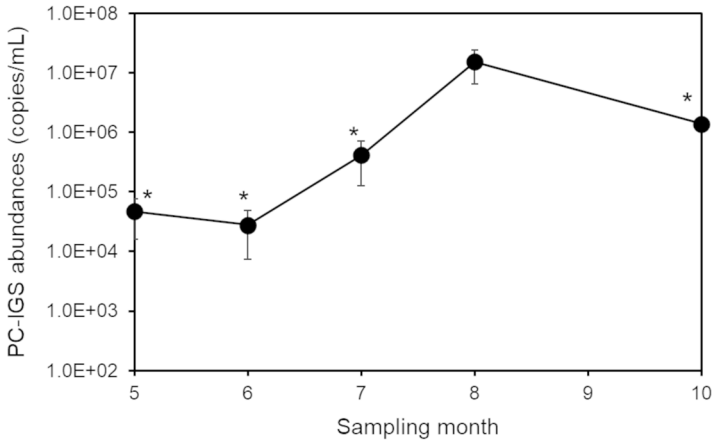

FIG 1 Seasonal changes in total abundances of *Microcystis aeruginosa* in the environment. Total abundance of *M. aeruginosa* was determined by quantitative PCR analysis. Error bars indicate standard deviation. *, Significant differences in the abundance compared with that in August ($P < 0.05$ by Tukey-Kramer test): in May ($P = 0.021$), June ($P = 0.021$), July ($P = 0.024$), and October ($P = 0.036$).

copies/mL) (*P* value, 0.036; Fig. 1). Thus, the intensity of the *Microcystis* bloom increased from early summer to autumn at Hirosawanoike Pond.

We further conducted *Microcystis* ITS amplicon analysis to monitor seasonal changes in their abundances at the intraspecies level in the environment. Our sampling of the *Microcystis* bloom generated a total of five amplicon samples from the Hirosawanoike Pond (Table S1 in the supplemental material). A total of 1,169,183 paired reads were obtained from these environmental samples (Table S1). After the quality control processes, an average of 183,596 merged reads were used for *Microcystis* ITS amplicon analysis (Table S1). On average, 105,762 *Microcystis* ITS sequences were extracted by using the ITS database derived from 159 *Microcystis* isolates (Table S1). These ITS amplicon sequences were largely divided into three groups (ITS types I to III), in accordance with the ITS phylotyping of *Microcystis* strains in previous studies (data not shown) (13, 33).

The *Microcystis* ITS I phylotype (14 operational taxonomic units [OTUs]) was the dominant phylotype in the environment (67 to 88% of total abundances) over the sampling period except in June (Fig. 2). The *Microcystis* ITS II phylotype (2 OTUs) accounted for 20 to 34% of total abundances from May to July and then became less abundant (0.4 to 2.9%) from August to October (Fig. 2). The *Microcystis* ITS III phylotype (5 OTUs) was present at a low abundance (3.2 to 13%) over the sampling period; however, its abundance rapidly increased up to 39% and 28% of total abundances in June and August, respectively (Fig. 2). Also, the standard deviation in the number of each ITS type reads per total assigned reads was lowest in June (Fig. 2).

Design of real-time PCR primers for *Microcystis* viruses with different host ranges. To investigate the relationships between the dynamics of *M. aeruginosa* and its broad-host-range viruses, we next identified the most abundant virus with a broad host range through the recruitment of virome reads collected in a previous study (23). Relative abundances of 4 broad-host-range viruses and 13 narrow-host-range viruses including Ma-LMM01 and MaMV-DC ranged from 31.5 to 50.1 and from 13.1 to 60.6 fragments per kilobase of exon per million mapped reads (FPKM) values, respectively (Fig. S1). We selected MVGF_NODE331 possessing the fourth most abundant spacers (23) as a target broad-host-range virus that was the most abundant in the environment. The narrow-host-range virus Ma-LMM01 was used for comparison, for which the quantification method was already established. This virus was the least abundant in the environment. Hence, we also selected MVGF_NODE620 as the most abundant target virus with a narrow host range.

Thereafter, the specific real-time PCR primer sets were designed to detect and quantify the broad-host-range virus MVGF_NODE331 and narrow-host-range virus MVGF_NODE620, respectively. For MVGF_NODE331 quantification, we checked the nucleotide diversity of the terminase gene through the recruitment of environmental

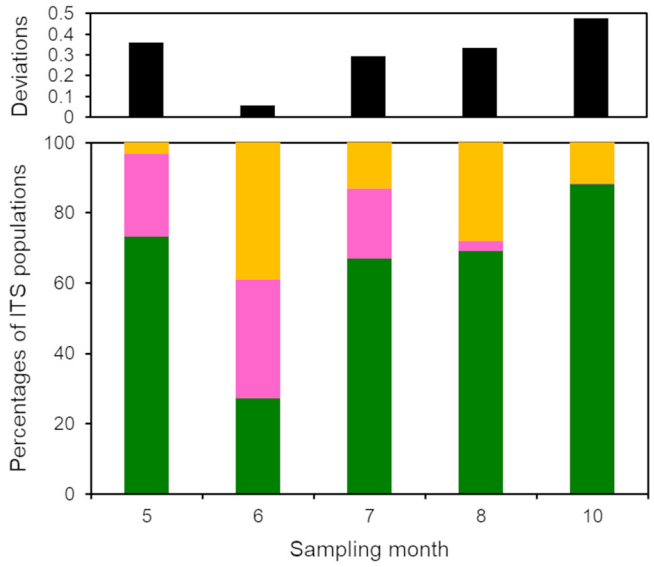

FIG 2 Temporal changes in abundances of *Microcystis* populations based on internal transcribed spacer (ITS) type in the environment. The percentages of *Microcystis* ITS I to III populations are shown in green, pink, and yellow, respectively. The top represents the standard deviations in the number of each ITS type reads per total assigned reads.

sequences. As a result, we found a single nucleotide polymorphism (SNP) located at 608 bp despite its low genetic diversity (Fig. 3). Therefore, we used the degenerate primers including the SNP region in the following experiments to comprehensively quantify MVGF_NODE331 and its close relatives (Table 1). We confirmed the SNP region in the terminase gene products by Sanger sequencing peak. Meanwhile, no nucleotide polymorphisms were included in the primer region of the PadR family transcriptional regulator for MVGF_NODE620 quantification (Fig. 3 and Table 1). A BLAST search with the primer sequences showed no genomic cross-reactivity with other viruses in the current database as well as the assembled viral database from the Hirosawanoike Pond (23). Both primer pairs could amplify a single specific product, which was confirmed by gel electrophoresis (Fig. S2) and Sanger sequencing (data not shown). The amplification efficiencies of the qPCR assay targeting for the broad- and narrow-host-range viruses were 110% and 112%, respectively ($R^2 \geq 0.98$; Fig. S3).

Changes in abundance of *Microcystis* viruses with different host ranges. Finally, we investigated the ecological dynamics of each *Microcystis* virus using viral fractions collected during the same sampling period to reveal differences in the relationships with total abundance and intraspecies population composition of *M. aeruginosa*. The broad-host-range virus MVGF_NODE331 decreased from 4.67×10^5 copies/mL in May to 3.19×10^3 copies/mL in June and then gradually increased up to 2.82×10^5 copies/mL in October (Fig. 4). The narrow-host-range virus MVGF_NODE620 did not markedly fluctuate over the sampling period (9.23×10^2 to 4.04×10^3 copies/mL) (Fig. 4). Likewise, *Microcystis* virus Ma-LMM01 with a narrow host range did not change in abundance and showed lower abundance than that of MVGF_NODE620 in the environment (1.28×10^2 to 6.34×10^2 copies/mL) (Fig. 4), which is consistent with FPKM value described above. Thus, the broad-host-range virus tended to be more dominant than the other two narrow-host-range viruses at the Hirosawanoike Pond over the sampling period except for June (Fig. 4). Meanwhile, an analysis of variance (ANOVA) test detected significant differences (*P* value, 0.034), but the Tukey-Kramer test for multiple comparisons did not show a significant difference among each data.

DISCUSSION

This is the first report focusing on the relationship between the ecological dynamics of viruses and changes in total host abundance and population composition in terms

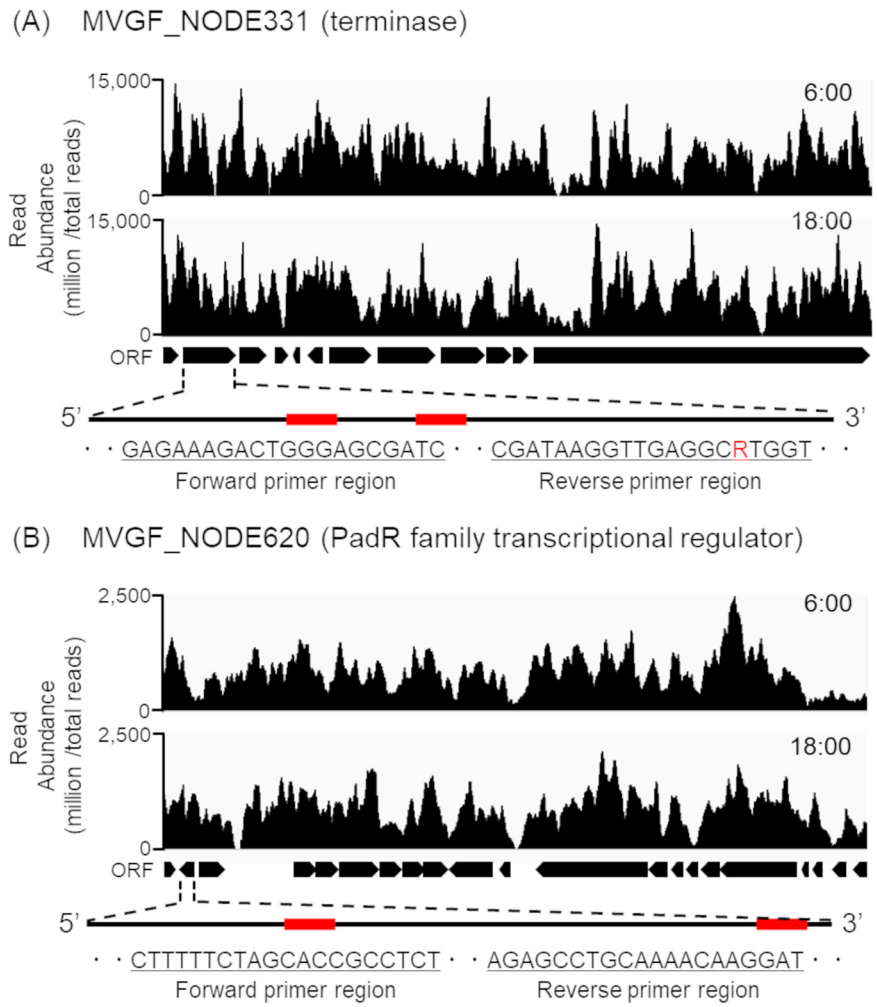

FIG 3 Virome read mapping pattern and nucleotide polymorphisms of the targeted *Microcystis* viral genomic fragments. (A) MVGF_NODE331. (B) MVGF_NODE620. Each viral names were designated in a previous study (23). The top and bottom of each virus represent the read mapping patterns derived from the sample collected at 06:00 and 18:00 in the previous study (23). The visualization and normalization of read abundances were conducted for each targeted virus by the Integrative Genomics Viewer function (43). Red rectangles indicate the position of target region in each gene.

of assumed host range differences. Our results using real-time PCR assays revealed that the abundance of the broad-host-range virus MVGF_NODE331 gradually increased over the sampling period, in proportion to the increase in total *Microcystis* abundance (Fig. 1 and 4). At this time, as supported by the standard deviation, the dominant ITS type of the *Microcystis* population temporarily declined to approximately equal rates to those of the other ITS type populations in June (Fig. 2); however, MVGF_NODE331 maintained its abundance in the environment at the same level as that in July (Fig. 4). Thus, the ecological dynamics of MVGF_NODE331 coincided with that of the whole host community regardless of the population composition, suggesting that broad-host-range viruses can proliferate in diverse host strains in the environment.

In contrast, both narrow-host-range viruses MVGF_NODE620 and Ma-LMM01 showed markedly lower abundance than that of the broad-host-range virus (Fig. 4). Also, these narrow-host-range viruses did not markedly fluctuate over the sampling period even though the total *Microcystis* abundance increased and the host population composition largely changed in June (Fig. 1, 2, and 4). However, previous studies indicated that these narrow-host-range viruses could rapidly increase or become temporarily dominant in the environment. For example, *Microcystis* virus Ma-LMM01 rapidly increased up to 1.1×10^4 copies/mL

TABLE 1 Primer sets for sequencing and real-time PCR assay used in this study

Primer	Sequence (5′ to 3′)[a]	References
188F	GCTACTTCGACCGCGCC	Yoshida et al. (45)
254R	TCCTACGGTTTAATTGAGACTAGCC	Yoshida et al. (45)
MITSamp-F	TCGTCGGCAGCGTCAGATGTGTATAAGAGACAG AAGGGAGACCTAATTCVGGT	Yoshida et al. (38)
MITSamp-R	GTCTCGTGGGCTCGGAGATGTGTATAAGAGACAG TTGCGGTCYTCTTTTTTGGC	Yoshida et al. (38)
g91DF1	CTGGGGTAATCAAGTTA	Kimura et al. (44)
g91DR3	CGGGTGGRGTTRMAYCYRCG	Kimura et al. (44)
MVGF331-F	GAGAAAGACTGGGAGCGATC	This study
MVGF331-R	ACCAYGCCTCAACCTTATCG	This study
MVGF620-F	CTTTTTCTAGCACCGCCTCT	This study
MVGF620-R	ATCCTTGTTTTGCAGGCTCT	This study

[a]Underline indicates overhang adapter sequence according to an Illumina MiSeq amplicon sequencing protocol.

in Lake Mikata (27). Likewise, the narrow-host-range virus MVGF_NODE620 showed the highest relative abundance at Hirosawanoike Pond in 2017 (Fig. S1) (23). Thus, the narrow-host-range viruses are thought to be prevalent if the specific host strain becomes dominant and thereby proliferates in the cells. This insight is also partly supported by the data that narrow-host-range viruses exhibited a broader range of FPKM values than that of the broad-host-range viruses (Fig. S1).

The results obtained in this study further indicated that *M. aeruginosa* could increase abundance and sustain dense bloom even under the increase of infection by the broad-host-range virus (Fig. 1 and 4). One of the reasonable explanations for the observations is that highly abundant and diverse antiviral mechanisms confer resistance to coexistence with its viruses under a negative frequency-dependent selection by viral infection. Indeed, *Microcystis* populations with different CRISPR spacers oscillated during the bloom, suggesting that this antiviral mechanism is one of the key factors in maintaining the population size under selective pressure (31). Likewise, it was proposed that nutrient loading and virion accidental methylation drive the excessive accumulation of restriction-modification (RM) system in the *Microcystis* genome, thereby allowing them with different sets of RM systems to coexist under the increased viral contact rate (11). The observation that *Microcystis* antiviral genes were expressed at the time of viral multiplication in the environment (23) also supported the importance of diverse antiviral mechanisms for the coexistence with viruses.

In conclusion, our data sets revealed differences in ecological dynamics between broad- and narrow-host-range viruses when the total abundance and population composition of

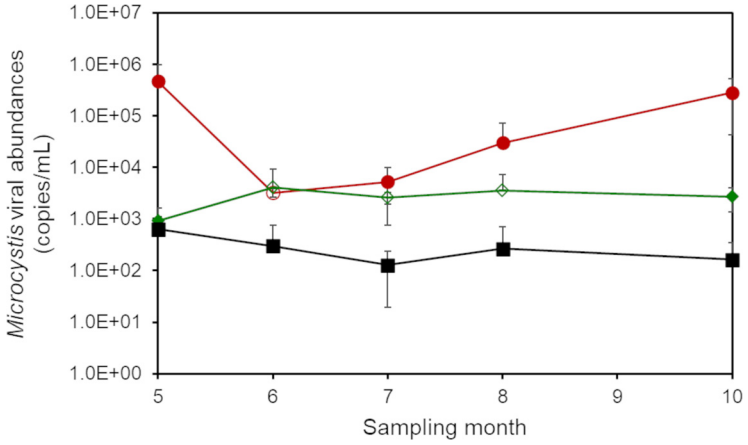

FIG 4 Temporal changes in abundances of the targeted *Microcystis* viruses including Ma-LMM01 in the environment. Ecological dynamics of MVGF_NODE331, MVGF_NODE620, and Ma-LMM01 are shown in red, green, and black, respectively. The *y* axis represents the average copy numbers of each target gene in triplicate samples (except for the samples shown by open symbols, $n = 2$). Error bars indicate standard deviation.

M. aeruginosa were changed. These results will help our understanding of the coexistence of *M. aeruginosa* with viruses with different host ranges and provide insight into the potential importance of highly abundant and diverse antiviral mechanisms for expanding and maintaining the bloom.

MATERIALS AND METHODS

Sampling. Seasonal freshwater samples were collected from the surface at an offshore point at Hirosawanoike Pond (35° 026′ N, 135° 690′ E) once per month from May to October 2016 except for September. For the amplicon analysis, the samples (100 mL) were gently sonicated followed by centrifugation at 3,000 rpm for 10 min. Cell pellets were stored at −20°C until DNA extraction. For quantification of viral abundance for each virus, 1.5 L of freshwater samples was prefiltered through a 142-mm 3.0-μm pore-size polycarbonate membrane filter (Millipore) and then filtered through 0.22-μm pore-size polycarbonate membrane filters or Sterivex units (Millipore). The filtrates (15 mL) were ultracentrifuged at 106,978 × *g* for 1.5 h, followed by resuspension in 200 μL of virus-free water and storage at −80°C.

Amplicon library preparation and sequencing. Genomic DNA extraction from the cell pellets was performed using a combination of the potassium xanthogenate-sodium dodecyl sulfate and phenol-chloroform/isoamyl alcohol procedures as described previously (34, 35). The extracted DNA was used for the following PCR as a template. *Microcystis* ITS region was amplified using specific primer sets MITS-F and MITS-R designed in a previous study (36) with 5′-end overhang adapter sequences according to an Illumina MiSeq amplicon sequencing protocol (Table 1). The resulting amplicons were purified using Agencourt AMPure XP beads (Beckman Coulter) according to the manufacturer's instructions. Amplicon libraries were sequenced using a MiSeq reagent kit v3 (2 × 300-bp read length; Illumina).

Amplicon data processing. The adaptor sequences of the raw sequence reads were automatically removed by the Illumina MiSeq system, whereas the primer region was trimmed by VSEARCH 2.9.1 (37). The quality of each raw sequence file was checked using FastQC (https://www.bioinformatics.babraham.ac.uk/projects/fastqc/). Trimmomatic v0.38 (38) was used to remove ambiguous and low-quality reads by scanning the reads with a 50-base-wide sliding window (quality score threshold = 20). The trimmed reads were merged using VSEARCH 2.9.1 with default parameter (37). After that, we removed the merged reads that were shorter than 200 bp, included "N" nucleotides, or showed quality scores <20. Chimera sequences were also removed using VSEARCH 2.9.1 (37). The remaining merged reads were clustered into OTUs using VSEARCH 2.9.1 with a sequence identity threshold of 100% (37), and then singleton OTUs were discarded at this stage. The representative sequences of the remaining OTUs were assigned to the ITS database collected from 159 *Microcystis* isolates in the current database including a previous study (13) (e-value threshold, 1.0×10^{-5}). The assigned *Microcystis* ITS sequences were aligned using the MAFFT program version 8.2.12 (39) and trimmed with trimAl version 1.4.1 (40). A maximum likelihood (ML) phylogenetic tree was constructed using RAxML version 8.2.12 (41). Bootstrap resamplings were conducted with 100 replications in the ML phylogenetic tree construction. The relative abundance of each *Microcystis* ITS type was calculated as a percentage of total *Microcystis* ITS sequences in a sample.

Selection of the target viruses. For selection of the target viruses, we referred to the abundances of each *Microcystis* viruses revealed through a metagenomic approach in a previous study (23). Briefly, the quality-controlled reads were aligned to the metagenome-assembled *Microcystis* viral genomes (23) including *Microcystis* virus Ma-LMM01 using Bowtie 2 (42) with the option "-score-min L,0,-0.6." The virome read abundances were normalized as fragments per kilobase of exon per million mapped reads (FPKM). We selected the most abundant broad- and narrow-host-range viruses as the target viruses (23).

Primer design and PCR amplification. The specific primers for the broad- and narrow-host-range viruses were designed to amplify a 133-bp region of the terminase coding gene and 194-bp region of PadR family transcriptional regulator coding gene, respectively (Table 1). These genes are not shared within the same *Microcystis* viral group. Also, we mapped virome reads collected at 18:00 on 19 October and 06:00 on 20 October 2017 in a previous study onto the target viral genomes under the same conditions as described above, visualized the read mapping patterns with the Integrative Genomics Viewer (43), and then the degenerate primer sets were designed based on the environmental sequences of primer regions (Table 1). Thereafter, these sequences were queried against the National Center for Biotechnology Information (NCBI) nonredundant (nr) and the previously assembled viral contig (≥10 kb) database (23) to ensure there were no nonspecific matches with other viruses.

Viral DNA was extracted from the filtered samples using the previously described xanthogenate-SDS method (34). PCR amplification with the primer sets was performed using TaKaRa PCR Thermal Cycler Dice Touch (TaKaRa Bio Inc.). The PCR mixture contained 12.5 μL of GoTaq Green Master Mix (Promega), 0.4 μM each primer, 1 μL of the extracted DNA, and virus-free water. Each PCR amplification consisted of an initial denaturation at 94°C for 1 min, followed by 30 cycles: 94°C for 30 s, 60°C for 30 s, 78°C for 30 s; with a final extension at 72°C for 5 min. After purification using the Wizard SV Gel and PCR Clean-Up System (Promega), the dilution series of PCR products were used as standard samples in the real-time PCR assay. The obtained products were confirmed to be a single band of the appropriate size by 2% gel electrophoresis (Fig. S2) and validated by the Applied Biosystems 3130 Genetic Analyzer (Thermo Fisher Scientific) (data not shown).

Quantification of the predicted broad- and narrow-host-range viruses. We conducted a real-time PCR assay with the designed primer sets to quantify the abundances of each target virus in the Hirosawanoike Pond from April to October 2016. The degenerate primer sets g91DF1 and g91 DR3 were also used for the quantification of *Microcystis* virus Ma-LMM01 (44), whereas the primer sets for

phycocyanin intergenic spacer (PC-IGS) were used for the quantification of *Microcystis* total abundance (32, 45) (Table 1). Each real-time PCR mixture contained 12.5 μL of TB Green Premix *Ex Taq* II (TaKaRa), 0.4 μM each primer, 2 μL of the extracted DNA, and virus-free water. These assays were performed using the Thermal Cycler Dice Real-Time System (TaKaRa) under the same amplification conditions as described above. A standard curve for each target virus was used for quantification and plotted using threshold cycle values. We confirmed a positive log-linear correlation between the C_T values and serial dilutions of each standard sample (terminase; R^2 = 0.990, PadR family transcriptional regulator; R^2 = 0.983) (Fig. S3). The specificity of each amplified standard sample was also verified by the dissociation curves. The detection ranges of terminase and PadR family transcriptional regulator sequences were approximately 1.0×10^2 to 10^7 and 1.0×10^2 to 10^8 gene copy numbers, respectively (Fig. S3). Host and viral abundance data were applied to an ANOVA test followed by the Tukey-Kramer test to estimate the significant differences, respectively ($P < 0.05$).

Data availability. The amplicon data sets were deposited in the DNA Data Bank of Japan (DDBJ) Sequence Read Archive under accession numbers DRR318264 to DRR318269.

SUPPLEMENTAL MATERIAL

Supplemental material is available online only.

SUPPLEMENTAL FILE 1, PDF file, 7.6 MB.

ACKNOWLEDGMENTS

This work was supported by Grants-in Aids for Scientific Research (S) (no. 21H05057) and (B) (no. 17H03850) from the Japan Society for the Promotion of Science (JSPS). This work was also partly supported by The Canon Foundation (no. 203143100025), JSPS Scientific Research on Innovative Areas (no. 16H06437), and the Bilateral Open Partnership Joint Research Project (Japan-Lithuania Research Cooperative Program) "Research on prediction of environmental change in Baltic Sea based on comprehensive metagenomic analysis of microbial viruses."

We declare that the research was conducted in the absence of any commercial or financial relationships that could be construed as a potential conflict of interest.

D.M. contributed to experiments and samplings, manuscript preparation, experimental design, and results discussion. N.Y. mainly conducted experiments and part of the *in silico* analysis. S.N. and A.S. supported the sampling and experiments. Y.S. contributed to manuscript discussion and revision. T.Y. contributed to the experimental design, results discussion, manuscript revision, and overall support for this study.

REFERENCES

1. Harke MJ, Steffen MM, Gobler CJ, Otten TG, Wilhelm SW, Wood SA, Paerl HW. 2016. A review of the global ecology, genomics, and biogeography of the toxic cyanobacterium, Microcystis spp. Harmful Algae 54:4–20. https://doi.org/10.1016/j.hal.2015.12.007.
2. MacKintosh C, Beattie KA, Klumpp S, Cohen P, Codd GA. 1990. Cyanobacterial microcystin-LR is a potent and specific inhibitor of protein phosphatases 1 and 2A from both mammals and higher plants. FEBS Lett 264:187–192. https://doi.org/10.1016/0014-5793(90)80245-E.
3. Nishiwaki-Matsushima R, Ohta T, Nishiwaki S, Suganuma M, Kohyama K, Ishikawa T, Carmichael WW, Fujiki H. 1992. Liver tumor promotion by the cyanobacterial cyclic peptide toxin microcystin-LR. J Cancer Res Clin Oncol 118:420–424. https://doi.org/10.1007/BF01629424.
4. Yoshizawa S, Matsushima R, Watanabe MF, Harada K, Ichihara A, Carmichael WW, Fujiki H. 1990. Inhibition of protein phosphatases by microcystis and nodularin associated with hepatotoxicity. J Cancer Res Clin Oncol 116:609–614. https://doi.org/10.1007/BF01637082.
5. Stewart I, Seawright AA, Shaw GR. 2008. Cyanobacterial poisoning in livestock, wild mammals and birds–an overview. Adv Exp Med Biol 619:613–637. https://doi.org/10.1007/978-0-387-75865-7_28.
6. Azevedo SMF, Carmichael WW, Jochimsen EM, Rinehart KL, Lau S, Shaw GR, Eaglesham GK. 2002. Human intoxication by microcystins during renal dialysis treatment in Caruaru-Brazil. Toxicology 181–182:441–446. https://doi.org/10.1016/s0300-483x(02)00491-2.
7. WHO. 2003. Cyanobacterial toxins: microcystin-LR in drinking water. Background document for preparation of WHO guidelines for drinking-water quality. World Health Organization, Geneva, Switzerland.
8. Dick GJ, Duhaime MB, Evans JT, Errera RM, Godwin CM, Kharbush JJ, Nitschky HS, Powers MA, Vanderploeg HA, Schmidt KC, Smith DJ, Yancey CE, Zwiers CC, Denef VJ. 2021. The genetic and ecophysiological diversity of Microcystis. Environ Microbiol 23:7278–7313. https://doi.org/10.1111/1462-2920.15615.
9. Makarova KS, Wolf YI, Snir S, Koonin EV. 2011. Defense islands in bacterial and archaeal genomes and prediction of novel defense systems. J Bacteriol 193:6039–6056. https://doi.org/10.1128/JB.05535-11.
10. Koonin EV, Makarova KS, Wolf YI. 2017. Evolutionary genomics of defense systems in archaea and bacteria. Annu Rev Microbiol 71:233–261. https://doi.org/10.1146/annurev-micro-090816-093830.
11. Papoulis SE, Wilhelm SW, Talmy D, Zinser ER. 2021. Nutrient loading and viral memory drive accumulation of restriction modification systems in bloom-forming cyanobacteria. mBio 12:e0087321. https://doi.org/10.1128/mBio.00873-21.
12. Kuno S, Yoshida T, Kaneko T, Sako Y. 2012. Intricate interactions between the bloom-forming cyanobacterium Microcystis aeruginosa and foreign genetic elements, revealed by diversified clustered regularly interspaced short palindromic repeat (CRISPR) signatures. Appl Environ Microbiol 78:5353–5360. https://doi.org/10.1128/AEM.00626-12.
13. Kuno S, Sako Y, Yoshida T. 2014. Diversification of CRISPR within coexisting genotypes in a natural population of the bloom-forming cyanobacterium Microcystis aeruginosa. Microbiology (Reading) 160:903–916. https://doi.org/10.1099/mic.0.073494-0.
14. Yang C, Lin F, Li Q, Li T, Zhao J. 2015. Comparative genomics reveals diversified CRISPR-Cas systems of globally distributed Microcystis aeruginosa, a freshwater bloom-forming cyanobacterium. Front Microbiol 6:394. https://doi.org/10.3389/fmicb.2015.00394.
15. Yoshida T, Takashima Y, Tomaru Y, Shirai Y, Takao Y, Hiroishi S, Nagasaki K. 2006. Isolation and characterization of a cyanophage infecting the toxic cyanobacterium Microcystis aeruginosa. Appl Environ Microbiol 72:1239–1247. https://doi.org/10.1128/AEM.72.2.1239-1247.2006.

16. Ou T, Li S, Liao X, Zhang Q. 2013. Cultivation and characterization of the MaMV-DC cyanophage that infects bloom-forming cyanobacterium Microcystis aeruginosa. Virol Sin 28:266–271. https://doi.org/10.1007/s12250-013-3340-7.
17. Naknaen A, Suttinun O, Surachat K, Khan E, Pomwised R. 2021. A novel jumbo phage PhiMa05 inhibits harmful Microcystis sp. Front Microbiol 12:660351. https://doi.org/10.3389/fmicb.2021.660351.
18. Jin H, Jiang YL, Yang F, Zhang JT, Li WF, Zhou K, Ju J, Chen Y, Zhou CZ. 2019. Capsid structure of a freshwater cyanophage Siphoviridae Mic1. Structure 27:1508–1516.e3. https://doi.org/10.1016/j.str.2019.07.003.
19. Lin W, Li D, Sun Z, Tong Y, Yan X, Wang C, Zhang X, Pei G. 2020. A novel freshwater cyanophage vB_MelS-Me-ZS1 infecting bloom-forming cyanobacterium Microcystis elabens. Mol Biol Rep 47:7979–7989. https://doi.org/10.1007/s11033-020-05876-8.
20. Watkins SC, Smith JR, Hayes PK, Watts JEM. 2014. Characterisation of host growth after infection with a broad-range freshwater cyanopodophage. PLoS One 9:e87339-8. https://doi.org/10.1371/journal.pone.0087339.
21. Cai R, Li D, Lin W, Qin W, Pan L, Wang F, Qian M, Liu W. 2022. Genome sequence of the novel freshwater Microcystis cyanophage Mwe-Yong1112-1. Arch Virol 167:2371–2376. https://doi.org/10.1007/s00705-022-05542-3.
22. Wang F, Li D, Cai R, Pan L, Zhou Q, Liu W, Qian M, Tong Y. 2022. A Novel freshwater cyanophage Mae-Yong1326-1 infecting bloom-forming cyanobacterium Microcystis aeruginosa. Viruses 14:2051. https://doi.org/10.3390/v14092051.
23. Morimoto D, Tominaga K, Nishimura Y, Yoshida N, Kimura S, Sako Y, Yoshida T. 2019. Cooccurrence of broad- and narrow-host-range viruses infecting the bloom-forming toxic cyanobacterium Microcystis aeruginosa. Appl Environ Microbiol 85:e01170-19. https://doi.org/10.1128/AEM.01170-19.
24. Yang F, Jin H, Wang X, Li Q, Zhang J, Cui N, Jiang Y-L, Chen Y, Wu Q-F, Zhou C-Z, Li W-F. 2020. Genomic analysis of Mic1 reveals a novel freshwater long-tailed cyanophage. Front Microbiol 11:484. https://doi.org/10.3389/fmicb.2020.00484.
25. Pound HL, Wilhelm SW. 2020. Tracing the active genetic diversity of Microcystis and Microcystis phage through a temporal survey of Taihu. PLoS One 15:e0244482-15. https://doi.org/10.1371/journal.pone.0244482.
26. Takashima Y, Yoshida T, Yoshida M, Shirai Y, Tomaru Y, Takao Y, Hiroishi S, Nagasaki K. 2007. Development and application of quantitative detection of cyanophages phylogenetically related to cyanophage Ma-LMM01 infecting Microcystis aeruginosa in fresh water. Microb Environ 22:207–213. https://doi.org/10.1264/jsme2.22.207.
27. Yoshida M, Yoshida T, Kashima A, Takashima Y, Hosoda N, Nagasaki K, Hiroishi S. 2008. Ecological dynamics of the toxic bloom-forming cyanobacterium Microcystis aeruginosa and its cyanophages in freshwater. Appl Environ Microbiol 74:3269–3273. https://doi.org/10.1128/AEM.02240-07.
28. Yoshida M, Yoshida T, Yoshida-Takashima Y, Kashima A, Hiroishi S. 2010. Real-time PCR detection of host-mediated cyanophage gene transcripts during infection of a natural Microcystis aeruginosa population. Microbes Environ 25:211–215. https://doi.org/10.1264/jsme2.ME10117.
29. Stough JMA, Tang X, Krausfeldt LE, Steffen MM, Gao G, Boyer GL, Wilhelm SW. 2017. Molecular prediction of lytic vs lysogenic states for Microcystis phage: metatranscriptomic evidence of lysogeny during large bloom events. PLoS One 12:e0184146. https://doi.org/10.1371/journal.pone.0184146.
30. McKindles KM, Manes MA, DeMarco JR, McClure A, McKay RM, Davis TW, Bullerjahn GS. 2020. Dissolved microcystin release coincident with lysis of a bloom dominated by Microcystis spp. in Western Lake Erie attributed to a novel cyanophage. Appl Environ Microbiol 86:e01397-20. https://doi.org/10.1128/AEM.01397-20.
31. Kimura S, Uehara M, Morimoto D, Yamanaka M, Sako Y, Yoshida T. 2018. Incomplete selective sweeps of Microcystis population detected by the leader-end CRISPR fragment analysis in a natural pond. Front Microbiol 9:425. https://doi.org/10.3389/fmicb.2018.00425.
32. Kimura S, Yoshida T, Hosoda N, Honda T, Kuno S, Kamiji R, Hashimoto R, Sako Y. 2012. Diurnal infection patterns and impact of Microcystis cyanophages in a Japanese pond. Appl Environ Microbiol 78:5805–5811. https://doi.org/10.1128/AEM.00571-12.
33. Otsuka S, Suda S, Li R, Watanabe M, Oyaizu H, Matsumoto S, Watanabe MM. 1999. Phylogenetic relationships between toxic and non-toxic strains of the genus Microcystis based on 16S to 23S internal transcribedspacer sequence. FEMS Microbiol Lett 172:15–21. https://doi.org/10.1111/j.1574-6968.1999.tb13443.x.
34. Tillett D, Neilan BA. 2000. Xanthogenate nucleic acid isolation from cultured and environmental cyanobacteria. J Phycol 36:251–258. https://doi.org/10.1046/j.1529-8817.2000.99079.x.
35. Yoshida M, Yoshida T, Takashima Y, Kondo R, Hiroishi S. 2005. Genetic diversity of the toxic cyanobacterium Microcystis in Lake Mikata. Environ Toxicol 20:229–234. https://doi.org/10.1002/tox.20102.
36. Yoshida M, Yoshida T, Satomi M, Takashima Y, Hosoda N, Hiroishi S. 2008. Intra-specific phenotypic and genotypic variation in toxic cyanobacterial Microcystis strains. J Appl Microbiol 105:407–415. https://doi.org/10.1111/j.1365-2672.2008.03754.x.
37. Rognes T, Flouri T, Nichols B, Quince C, Mahé F. 2016. VSEARCH: a versatile open source tool for metagenomics. PeerJ 4:e2584. https://doi.org/10.7717/peerj.2584.
38. Bolger AM, Lohse M, Usadel B. 2014. Trimmomatic: a flexible trimmer for Illumina sequence data. Bioinformatics 30:2114–2120. https://doi.org/10.1093/bioinformatics/btu170.
39. Katoh K, Misawa K, Kuma K-i, Miyata T. 2002. MAFFT: a novel method for rapid multiple sequence alignment based on fast Fourier transform. Nucleic Acids Res 30:3059–3066. https://doi.org/10.1093/nar/gkf436.
40. Capella-Gutiérrez S, Silla-Martínez JM, Gabaldón T. 2009. trimAl: a tool for automated alignment trimming in large-scale phylogenetic analyses. Bioinformatics 25:1972–1973. https://doi.org/10.1093/bioinformatics/btp348.
41. Stamatakis A. 2006. RAxML-VI-HPC: maximum likelihood-based phylogenetic analyses with thousands of taxa and mixed models. Bioinformatics 22:2688–2690. https://doi.org/10.1093/bioinformatics/btl446.
42. Langmead B, Salzberg SL. 2012. Fast gapped-read alignment with Bowtie 2. Nat Methods 9:357–359. https://doi.org/10.1038/nmeth.1923.
43. Robinson TJ, Thorvaldsdóttir H, Winckler W, Guttman M, Lander SE, Getz G, Mesirov PJ. 2011. Integrative genomics viewer. Nat Biotechnol 29:24–26. https://doi.org/10.1038/nbt.1754.
44. Kimura S, Sako Y, Yoshida T. 2013. Rapid Microcystis cyanophage gene diversification revealed by long and short-term genetic analyses of the tail sheath gene in a natural pond. Appl Environ Microbiol 79:2789–2795. https://doi.org/10.1128/AEM.03751-12.
45. Yoshida M, Yoshida T, Takashima Y, Hosoda N, Hiroishi S. 2007. Dynamics of microcystin-producing and non-microcystin-producing Microcystis populations is correlated with nitrate concentration in a Japanese lake. FEMS Microbiol Lett 266:49–53. https://doi.org/10.1111/j.1574-6968.2006.00496.x.